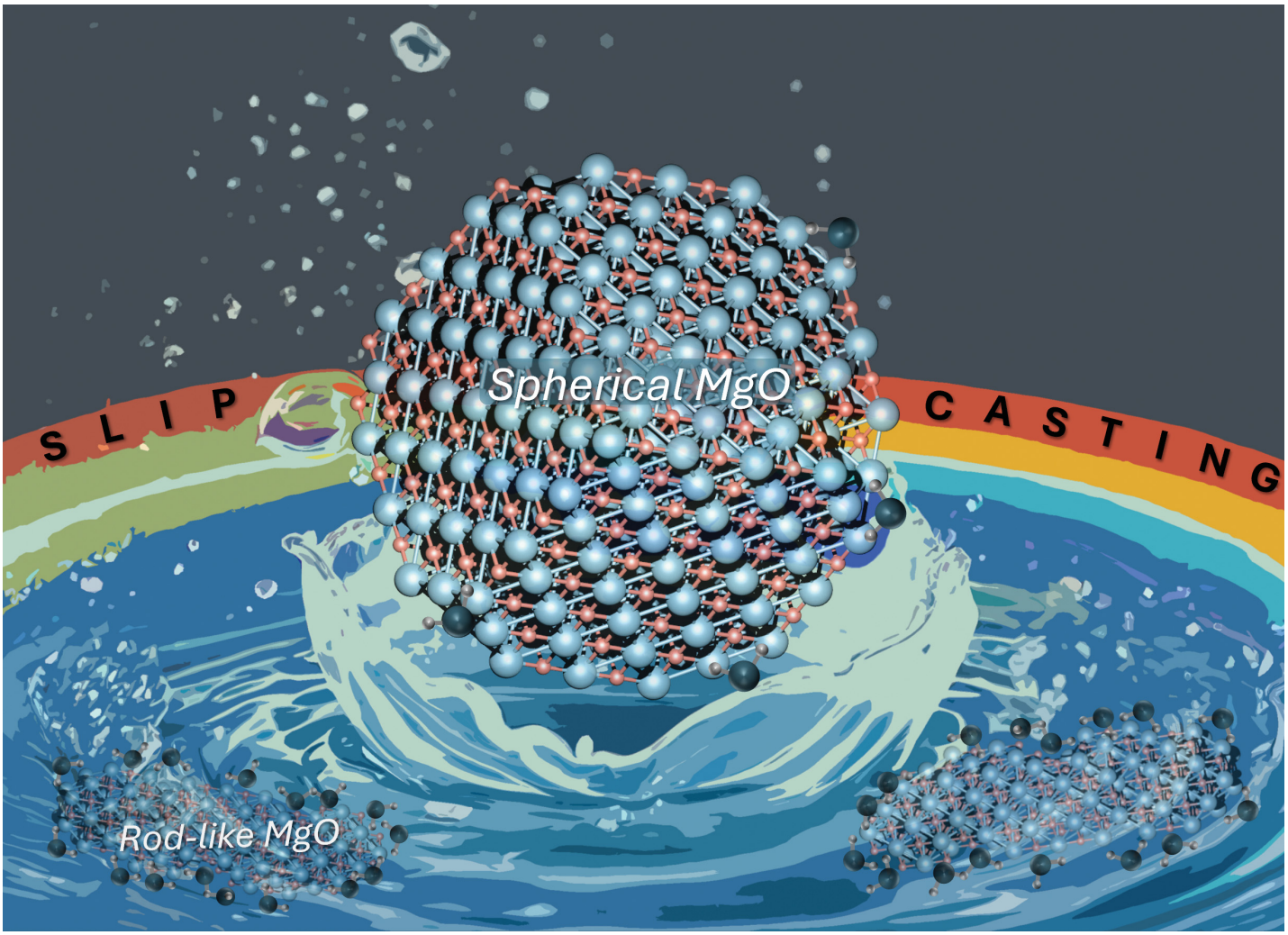

Showcasing discovery from collaborative research between University of Nottingham, Nottingham, UK and Almath Crucibles Ltd., Cambridge, UK, led by Dr Yu Yu and Professor George Zheng Chen.

Hydration control in the fabrication of high-density magnesia products *via* slip casting

In the slip casting process, rod-like fine MgO particles with numerous surface steps and defects undergo strong hydration and struggle to escape from the water. Conversely, larger spherical MgO particles exhibit reduced interaction with water and demonstrate excellent flowability, facilitating successful slip casting.

As featured in:

See George Z. Chen *et al.*, *Mater. Adv.*, 2024, **5**, 6830.

ROYAL SOCIETY OF CHEMISTRY

rsc.li/materials-advances

Registered charity number: 207890

Materials Advances

ROYAL SOCIETY OF CHEMISTRY

PAPER

View Article Online
View Journal | View Issue

Cite this: *Mater. Adv.*, 2024, 5, 6830

Hydration control in the fabrication of high-density magnesia products *via* slip casting

Yu Yu, [ab] Arkadiusz Gargala,[b] Michael Misson[b] and George Z. Chen [*a]

Received 26th September 2023,
Accepted 26th June 2024

DOI: 10.1039/d3ma00768e

rsc.li/materials-advances

To tackle the hydration problem in magnesia (MgO) aqueous suspension during slip casting fabrication, we explored the casting performance of four distinct MgO slips. Through the comparison of properties and performance between aqueous and organic MgO slips, we introduced criteria for selecting the appropriate suspension medium to prepare a good MgO slip. Moisture absorption in raw MgO powders leading to $Mg(OH)_2$ formation was observed, undetectable by X-ray diffraction (XRD) but identified through thermogravimetric analysis (TGA). Moisture release occurred at temperature < 100 °C, followed by loosely bound water release between 160 °C and 310 °C, and then $Mg(OH)_2$ decomposition occurred at 310 °C to 430 °C, constituting 1.05, 1.66, and 1.34 wt%, respectively. Subjecting raw powders to pre-firing at 1000 °C led to the formation of larger MgO particles, characterised by a D50 value twice that of the previous size. This transformation shifted their morphology from random rods to more durable spherical shapes, thereby improving their resistance to hydration when subjected to wet ball milling with water. Pre-firing MgO at 1000 °C resulted in a favourable aqueous slip, enabling problem-free casting of small-sized products with high density and purity.

1. Introduction

Magnesia (MgO) has a maximum working temperature of 2200 °C, surpassing the 1750 °C limit of the most widely used refractory, alumina (Al_2O_3). Its superior chemical stability makes it inert to metals,[1] slags,[2] and superconducting compounds,[3] thereby it plays a crucial role in various applications including high-temperature molten salt electrolysis,[4] metal smelting, and slag processing.[5] The impressive chemical stability of MgO arises from the higher affinity of magnesium to oxygen compared to aluminium. This characteristic prevents the oxygen in MgO from being seised by other active metallic substances like aluminium, titanium, iron, and silicon.

Unlike Al_2O_3, which can be readily fabricated in high purity and density through casting of an aqueous slip, the fabrication of MgO products is challenging due to its inherent tendency to hydrate when formulating an aqueous slip. MgO hydration has been extensively reported in literature studies,[6–9] which arises when water molecules including those in the vapour form react with MgO primarily on its surface, forming an $Mg(OH)_2$ layer.[10] This layer can dissolve in water, revealing fresh MgO surfaces for further reaction. As $Mg(OH)_2$ has lower density than MgO, this hydration process causes volume expansion,[11] leading to increased viscosity in the slip, which presents a significant challenge in slip casting MgO products. A similar issue caused by hydration is found in the casting of aqueous CaO slips. To address this, some researchers use $Ca(OH)_2$ instead of CaO to make an aqueous slip, avoiding the hydration issue.[12,13] $Ca(OH)_2$ undergoes decomposition during sintering, resulting in significant shrinkage. This characteristic could necessitate extra care in tool design and production, particularly when scaling up the product size, unlike other oxide ceramics. This work focuses on controlling the hydration of MgO slips rather than using $Mg(OH)_2$.

Research on slip casting MgO is relatively rare compared to other ceramic oxides. Most studies involve MgO as an additive or component in mixed oxides, rather than focusing on high-purity MgO, *e.g.*, $MgO–Al_2O_3$,[14,15] $MgO–ZrO_2–Al_2O_3$,[16] and $MgO–Y_2O_3$[17,18] mixtures with MgO typically constituting no more than 50 wt%. In this work, we focus on producing high-purity (>95 wt%) MgO products. Previous reports on this level of purity have been found, as discussed below.

In 1939, Thompson and Mallett published the earliest well-recognised article on slip casting MgO. They observed that MgO slips were sticky and rubbery compared to other refractories, resulting in soft, weak castings that adhered tightly to the mould. Despite water being the most common dispersion medium in slip casting, their experiments led them to conclude that aqueous slips were unsuitable for casting MgO crucibles.[19]

In 1957, Stoddard *et al.* reported slip casting a water suspension of coarse MgO powders (particle size ranging from 44 to 500 μm). Despite the large particles slowing down the surface

[a] *Department of Chemical and Environmental Engineering, University of Nottingham, Nottingham NG7 2RD, UK. E-mail: George.Chen@nottingham.ac.uk*
[b] *Almath Crucibles Ltd., Newmarket, Cambridge CB8 9NE, UK*

hydration, the density after sintering at 1800 °C was only 81–84% of the theoretical value.[20]

They reported a process improvement in 1963. By chilling the water slip in a 2–10 °C fridge and extending ball milling to 72 hours, the MgO particle size was reduced, and a 95% theoretical density was achieved after sintering at 1600 °C. However, shortening milling to 30 hours may require sintering at 2200 °C to achieve the same density.[21] In the same year, Whiteway discovered that extending the milling time of MgO powders (with a particle size less than 400 μm) from 14 hours to 100 hours resulted in the MgO slip gradually picking up alumina impurities from the milling jar or grinding balls.[22]

Since the 1990s, researchers have explored different methods for preparing an aqueous MgO slip to minimise hydration. Skomorovskaya *et al.* successfully controlled hydration by wet milling MgO in a dispersion medium containing a colloidal component in 1991. They separated the colloidal component through centrifugation and replaced it with water, although the specific component used was not mentioned in their report.[23] This multi-step process may not be suitable for industrial production compared to directly casting the MgO slip. In 2011, Mondy *et al.* treated MgO particles with carboxylic and dicarboxylic acids to create particle-stabilised oil/water emulsions, which still contained $Mg(OH)_2$.[24] In the same year, Silva *et al.* studied the effects of alumina and silica on the hydration behaviour of MgO in casting aqueous slips. They found that the presence of alumina hardly reduces hydration but adding 16.7–25% silica content to MgO could help inhibit cracking related to the hydration product. They also pointed out that this high amount of silica can negatively affect certain product properties.[25]

Thompson and Mallett successfully cast MgO from a suspension of finely ground MgO in 100% ethanol, after concluding that MgO could not be cast from the aqueous slip.[19] Since then, several reports on slip casting MgO have utilised ethanol.[18,22,26,27] Other organic solvents such as toluene, methanol, 2-butanol, 1-propanol, and isopropanol have also been used in slip casting MgO.[24,26]

When ball milling nano and sub-micron MgO powders in these organic solvents, the resulting slips exhibited excellent flowability due to significantly reduced hydration. Sintering at 1650 °C readily achieved over 95% of the theoretical density. However, casting with organic solvent based MgO slips is slower than that with aqueous slips. Stoddard *et al.* achieved a 3 mm wall thickness in 6 minutes with an aqueous MgO slip containing 80 wt% MgO,[20] while Oumizono *et al.* reported wall thicknesses of 3.78 mm, 2.54, 2.06, 1.57, and 1.24 mm within 2 hours for slips of 75 wt% MgO in isopropanol, methanol, 2-butanol, ethanol, and 1-propanol, respectively.[26]

Furthermore, the water content in an organic MgO slip can significantly impact its properties. Whiteway *et al.* studied the influence of water on MgO ethanol slips. They discovered that when the MgO concentration exceeded 65 wt%, adding 1.0–1.5% water (relative to the total slip weight) led to slip gelling, resulting in a sharp increase in viscosity.[28] Excluding water from MgO ethanol (or other organic solvents) slips appears to be essential for casting MgO successfully.

Nowadays, selecting water as a solvent still requires careful consideration, even when using MgO as an additive or a composite component. Bagaria reported the use of water as a solvent in 2012 when preparing an alumina slip with low concentrations of MgO dopants (up to 0.5 wt%).[14] For slip casting some MgO-containing mixtures such as MgO–Y_2O_3, ethanol is often preferred over water, and special techniques such as slip casting under pressure are employed to facilitate the process, as demonstrated by Mahmoudabad *et al.* in 2019.[18] Sometimes, ethanol is preferred even in casting high-purity Y_2O_3, as reported by Xu *et al.* in 2017.[29]

Presently, the production of high-purity and high-density MgO products predominantly relies on the isostatic pressing method, despite its high cost and the challenges associated with designing elastomeric bags. Considering the advantages of slip casting—a cost-effective manufacturing approach to making ceramics, applicable to a wide range of materials, and suitable for creating products with complex designs—the investigation of controllable manufacture of MgO products *via* slip casting holds significant importance.

This study, as the first of its kind, aims to addressing the challenges of casting aqueous MgO slips to produce high-density (>95% of the theoretical value) and high-purity (>95 wt%) MgO products. Four distinct MgO slips were formulated, and their casting behaviour was examined under identical experimental conditions. By testing different solvents and employing powder management strategies, we effectively controlled hydration in casting an aqueous MgO slip, ultimately fabricating MgO crucibles in the designated shapes and dimensions. These findings hold promise for the cost-effective manufacture of high-quality MgO products across various applications.

2. Experimental

2.1. MgO slip formulation and casting

MgO powder (97%, Celtic Chemicals UK, specific surface area of 31.68 $m^2\ g^{-1}$) along with the chosen solvent, deflocculant (DISPEX AA 4140, BASF plc Bradford, UK), and yttria powder (Minchem UK, specific surface area of 2.73 $m^2\ g^{-1}$), were blended within a 500 mL plastic bottle (Nalgene). Subsequently, the slips underwent a ball milling process lasting 16 hours at a milling rate of 60 rpm, utilising alumina grinding balls.

Four distinct recipes were employed in the creation of MgO slips, designated as slip I, slip II, slip III, and slip IV, with specific details outlined below.

Slip I: 100 g of MgO powder, 77 g of deionised water, 0.64 mL of deflocculant, and 1.2 g of yttria (Y_2O_3) powder.

Slip II: 100 g of MgO powder, 67 g of isopropanol alcohol (industrial 99.9%, Trade Chemicals Ltd, UK), 0.64 mL of deflocculant, and 1.2 g of Y_2O_3 powder.

Slip III: 100 g of MgO powder, 67 g of acetic acid (99%, Sigma Aldrich), 0.64 mL of deflocculant, and 1.2 g of Y_2O_3 powder.

Slip IV: MgO powder was pre-fired at 1000 °C for 4 hours, and then was used to make a slip following the recipe outlined in slip I.

Since the hydration of MgO is an exothermic reaction as shown in reaction (1) below, its rate can be affected by temperature. Thus, all ball milling processes were conducted in a refrigerated environment at a constant temperature of 5 °C. This temperature was specifically chosen to intentionally slow down the formation of $Mg(OH)_2$ and minimise its influence on slip viscosity.

$$MgO(s) + H_2O(g) \leftrightharpoons Mg(OH)_2(s)\ \Delta H = -81.02\ kJ\ mol^{-1} \quad (1)$$

MgO slips were cast into plaster moulds specifically designed and manufactured by Almath Crucible Ltd. These plaster moulds are composed of $CaSO_4{\cdot}2H_2O$, which is formed by mixing $CaSO_4{\cdot}1/2H_2O$ (NEWCAST 96) and water at a weight ratio of 1.75 : 1. The freshly cast MgO green bodies were air-dried for a period of 2 days under ambient conditions. Subsequently, they were introduced into the furnace and subjected to sintering at 1610 °C, aiming at maximal densification.

A reference ZrO_2 slip was prepared by ball milling 260 g of zirconia powder (stabilised with 8 mol% yttria, Minchem UK, specific surface area of 7 $m^2\ g^{-1}$), 0.15 mL of deflocculant, and 100 g of deionised water for 10 hours at room temperature.

2.2. Characterisation

The phase identification of the raw MgO powder, pre-fired MgO powder, and fully dried MgO green bodies resulting from different slips was conducted using an X-ray diffractometer (Bruker AXS D8-Advance) equipped with a Cu Kα X-ray source (λ = 1.5406 Å). Data collection spanned the 2θ range of 10–80°, employing a step width of 0.02° and a holding time of 0.4 s. For phase identification in this study, the DIFFRAC EVA software (Bruker) and the PDF-2 2015 database from the International Centre for Diffraction Data (ICDD) were employed.

The morphologies of the starting powders and final products were analysed using JEOL 6490LV and JEOL 7100F field emission scanning electron microscopes (SEM). Both the secondary electron and the backscattered electron imaging modes were employed with a working distance of 10 mm.

The particle size distribution of MgO powders was analysed using both the Nano Measurer 1.2 software and SEM secondary electron imaging. The procedure encompassed the following steps: (1) importing SEM images into the Nano Measurer 1.2 software; (2) establishing the scale bar; (3) measuring the particle size (from corner to corner); and (4) generating a statistical analysis report. To facilitate the process, a small quantity of powder (~20 mg) was subjected to ultrasonic dispersion in 5 mL of acetone for a duration of 15 min. Subsequently, 30 μL of the suspension was applied onto the SEM sample holder and allowed to air-dry for 5 min under ambient conditions. In order to ensure an adequate deposition of powder particles, the aforementioned steps were repeated at least three times.

Specific surface areas of different oxide powders were determined by Brunauer-Emmett-Teller (BET) analysis (Micromeritics TriStar II 3020 Version 3.02).

Thermogravimetric analysis (TGA) of both the raw and pre-fired MgO powders was conducted using an SDT Q600 instrument from TA Instruments. For each analysis, a quantity of 10 to 20 mg powder was placed within an alumina TGA crucible, with a corresponding blank alumina TGA crucible serving as a reference. The heating rate employed was 10 °C min^{-1}, ranging from 20 to 1100 °C, with continuous air purging into and out of the chamber at a flow rate of 100 mL min^{-1}.

The viscosity of the MgO slip was determined using a model NDJ-8S Digital Rotary Viscometer, utilising a No. 1 spindle operating at 12 rpm, and the temperature of the slip was maintained at 5 °C.

The density of the sintered MgO products was measured using an analytical balance in combination with the Archimedes density kit (SARTORIUS ENTRIS II 224I and YDK03).

3. Results and discussion

3.1. Effects of MgO hydration on slip casting

After undergoing 16 hours of ball milling at 5 °C, slip I of MgO turned as thick as the ice cream, losing its ability to flow, and making it impossible to cast, as shown in Fig. 1(a). Ideally, for slip casting, the desired state of the slip should resemble that of milk, comparable to the state demonstrated in Fig. 1(b) featuring the zirconia slip. This milk-like zirconia slip can ensure the mould to be filled smoothly to capture all the details of the intended shape.

After undergoing a two-day drying process under ambient conditions, the initially consolidated slip I was manually ground into a powdered form using a pestle and mortar. The resulting powder underwent X-ray diffraction (XRD) analysis. Fig. 1(c) presents the XRD patterns for both the original raw MgO powder and the consolidated MgO obtained from slip I.

It was thought that the interaction between the MgO powder and water during the slip preparation initiated the formation of $Mg(OH)_2$. This is evident from the peaks observed at 2θ = 19.3°, 32.9°, 38.0°, 50.8°, and 58.8°, which align with the PDF No. 44-1482 for $Mg(OH)_2$. Additionally, the peaks located at 2θ = 29.1°, 33.9°, 48.5°, and 57.6° can be ascribed to the presence of Y_2O_3. Y_2O_3 possesses a cubic crystal structure, as illustrated in Fig. 2(f). In this study, Y_2O_3 was intentionally introduced into the MgO slip as an additive with the purpose of enhancing sintering behaviour. Sintering primarily involves processes such as densification and the elimination of pores, facilitated by the migration of matter (Mg^{2+} and O^{2-}) through lattice defects.

The formation of both Frankel defects and Schottky defects can occur within the MgO crystal lattice, as described by reactions (2) and (3). It is worth noting that the formation of these defects demands a substantial amount of energy.

$$Mg_{Mg}^{\times} \rightarrow Mg_i^{\bullet\bullet} + V_{Mg}'' \,(\text{Frankel defect}) \quad (2)$$

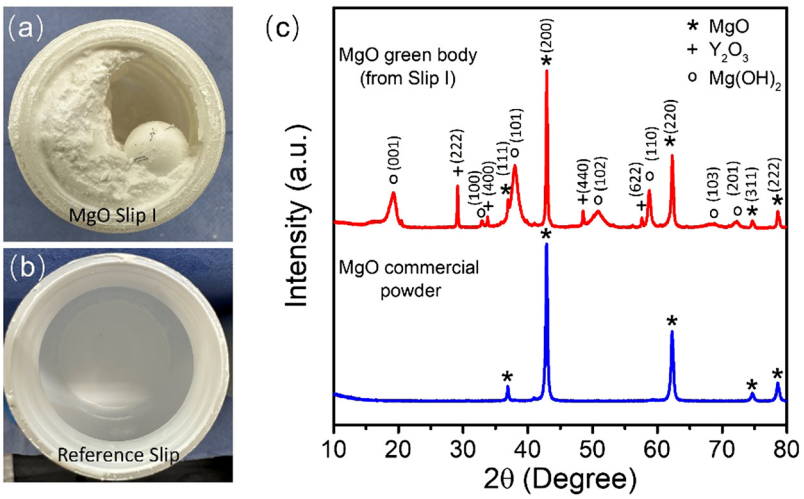

Fig. 1 Slip conditions and the phase composition of the resultant green body from MgO slip I. (a) Photograph of slip I. (b) Reference photograph of a typical zirconia slip. (c) XRD patterns of commercial MgO powder and the MgO green body originating from slip I. XRD diffraction peaks corresponding to MgO, Y_2O_3, $Mg(OH)_2$ are referenced with PDF No. 45-0946, 43-1036, and 44-1482, respectively.

$$\text{null} \rightarrow V''_{Mg} + V^{\bullet\bullet}_{O}\ (\text{Schottky defect}) \quad (3)$$

Frankel defects typically require an energy input within the range of 10.3 to 15.2 eV,[30–34] while Schottky defects require an energy input ranging from 6.8 to 7.5 eV.[35,36]

Furthermore, the diffusion coefficients for both Mg^{2+} and O^{2-} are notably low. At a temperature of 1800 °C, near the grain boundary, the diffusion coefficient is 1.0×10^{-11} cm^2 s^{-1} for Mg^{2+} and 1.4×10^{-10} cm^2 s^{-1} for O^{2-}.[37] These make it difficult to achieve effective densification during sintering. While MgO can only melt beyond 2800 °C, Y_2O_3 possesses a comparatively lower melting point, reduced by approximately 400 °C. Given the eutectic point in the Y_2O_3–MgO phase diagram at 2120 °C,[38] sintering at 1610 °C cannot result in the formation of a Y_2O_3–MgO solution. However, the presence of nano-sized Y_2O_3 particles (as shown in Fig. 2) could introduce a quasi-liquid phase during sintering at 1610 °C. Additionally, the unoccupied corner sites within the unit cell of Y_2O_3 (Fig. 2(f)) can serve as vacancies, facilitating the diffusion of O^{2-} along the grain boundaries of MgO. This aids in the transfer of matter and enhances densification.

Given that both Y_2O_3 and MgO have a cubic crystal structure, as shown in Fig. 2(c) and (f), and that the added amount of Y_2O_3 was as low as 1.2 wt%, the addition of Y_2O_3 should not adversely affect the properties of MgO, unlike silica or alumina additives.[25] As Y_2O_3 and MgO exhibit low solubility in each other, Y_2O_3 is distributed at the boundaries and restricts the abnormal grain growth of MgO during sintering,[39] leading to a uniform grain size, as shown in Fig. 2(g)–(i).

In earlier research, an MgO slip was successfully prepared using a 15-hour ball milling process at 16 °C. This involved mixing fused MgO powder with particle sizes of < 74 μm (fused MgO is produced by fusing in an electric arc furnace) and water, with a milling rate of 50 rpm.[40] In another similar study, slip formation through ball milling fused MgO powder (<74 μm) with water up to 72-hours was achieved at temperatures ranging from 2 to 10 °C.[21] Additionally, an MgO slip was formed by ball milling calcined MgO powder (149–355 μm) with water, employing temperatures below 35 °C for a duration of 16.5 hours.[41]

In our study, we observed a significant level of hydration during the ball milling of the commercial MgO powder (D50 of 0.79 μm) with water for 16 hours at 5 °C. The resulting slip differs from those produced in the aforementioned research, because the kinetics of reaction (1) can be greatly influenced by distinct MgO powders possessing varying properties such as particle size and specific area. Creating fused powders from this commercial MgO product demands a high energy input, and larger particles require extended ball milling with water to address densification issues during sintering. Therefore, we initiated research to explore solutions for casting this commercial powder, which will be detailed in the subsequent sections.

3.2. Modification of the MgO slip through solvent adjustment

Slip II was prepared by mixing the commercial MgO powder with isopropanol (iPrOH) as a replacement for water, aiming to prevent the formation of $Mg(OH)_2$. As shown in Fig. 3(a), slip II displayed good flowability, with a measured viscosity of 55.9 mPa s when the rotator speed was set to 12 rpm. XRD results from the MgO green body produced using slip II, as depicted in Fig. 3(c), provided evidence that changing the solvent from water to iPrOH effectively suppressed the emergence of $Mg(OH)_2$. This modification reduced the presence of $Mg(OH)_2$ to a level below the detection limit of XRD.

Fig. 3(h) schematically illustrates the hydration process of MgO for slip I, based on the studies conducted by different researchers that have focused on investigating water absorption and dissociation on the MgO surface using both experimental and first principles molecular dynamics simulations.[42–45] When water molecules are absorbed on the MgO (100) plane, which is the most exposed plane for MgO powders as confirmed

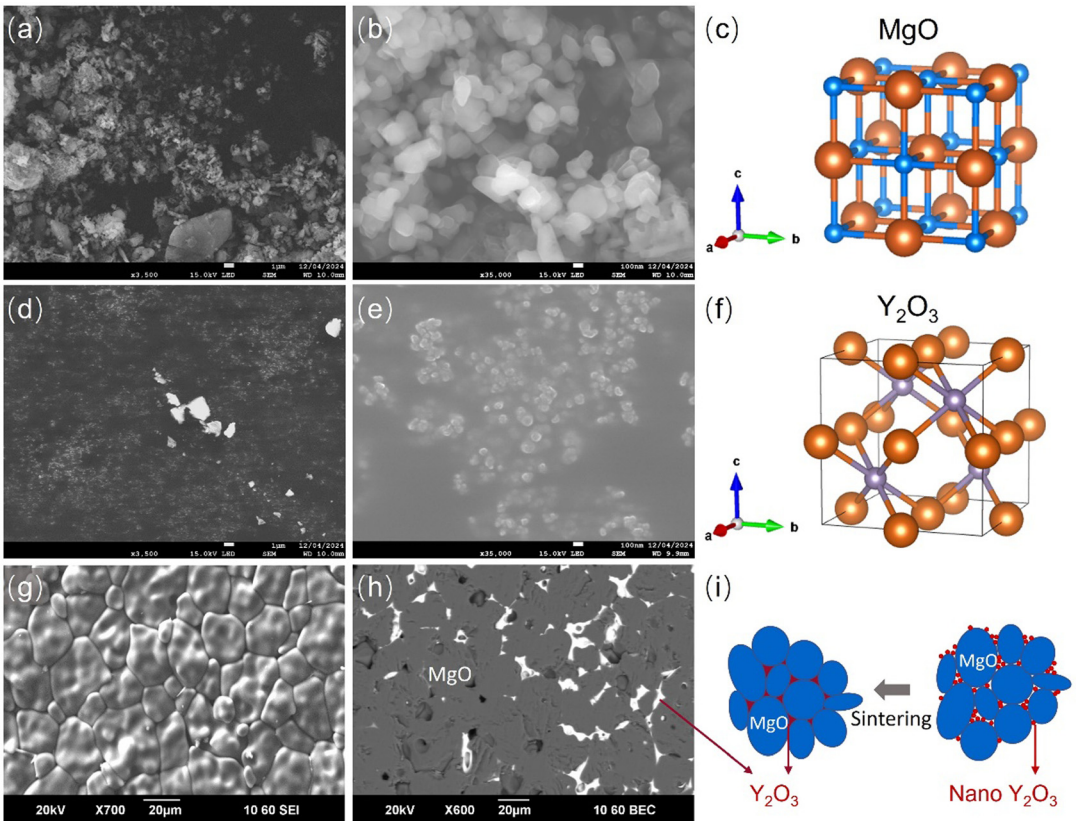

Fig. 2 Y_2O_3 enhanced sintering of MgO. Low- and high-magnification SEM images of the commercial MgO powder are shown in (a) and (b) respectively, while images of the Y_2O_3 powder are shown in (d) and (e). Crystal structure of (c) MgO (Z = 4 in the unit cell) and (f) Y_2O_3 (Z = 2). SEM secondary image (g) and backscattered image (h) of a MgO product sintered at 1610 °C with the addition of Y_2O_3. (i) Nano-sized Y_2O_3 additive is distributed on the surfaces of individual micron-sized MgO particles, resulting in a boundary distribution of Y_2O_3 during sintering.

by XRD analysis, a monolayer of water is formed. Strong hydrogen bonds are established within the water monolayer and between the water monolayer and the surface oxygen ions on the MgO (100) plane. These absorbed water molecules can undergo dissociation, transferring a proton to a surface lattice oxygen atom, leading to the formation of OH^- species which are oriented perpendicular to the interface, as illustrated in Fig. 3(h). Ding *et al.* also noted the presence of metastable OH^- arranged perpendicular to the interface, located slightly above the first water layer, which is not represented in Fig. 3(h). These OH^- species are formed when a water molecule forms hydrogen bonds with four neighbouring water molecules within the first water layer. Their proton of OH^- points toward the bulk water, while their associated protons are bound to the surface oxide ions. The formation of these OH^- species is linked to the strong basic nature of the MgO surface.[42]

In contrast to water, the hydrogen bonds between iPrOH molecules and the surface oxygen ions of the MgO substrate are significantly weaker. Additionally, the presence of the $(CH_3)_2$–CH– chain hinders the interaction between the iPrOH and the MgO surface, effectively preventing the formation of $Mg(OH)_2$. This promising slip was employed for casting MgO lids. Unexpectedly, a new issue arose during this process.

Due to its higher vapour pressure of 4.67 kPa compared to 2.34 kPa for water as indicated in Table 1, iPrOH exhibits a faster rate of evaporation into the atmosphere. Additionally, the plaster mould cannot absorb iPrOH as effectively as water. Moreover, the hydrogen bonding of MgO with iPrOH is weaker compared to that with water. These factors combined, resulting in faster inner surface drying than the outer surface. Given the delicate nature of MgO green bodies created from the iPrOH-based slip, this discrepancy in drying rates contributed to cracks forming on the inner surface, as illustrated in Fig. 4(a).

To test this hypothesis, two different methods were used to cast the MgO lids using slip II. In one case, the slip was cast directly, and the mould was left in ambient conditions. In the other case, after casting a plaster mould of the same shape and size was placed on top to enclose the space above slip II. This prevented the rapid evaporation of iPrOH. The outcomes aligned with the assumption, as illustrated in Fig. 3(d)–(g). The MgO lid without the cover exhibited several cracks on its surface, while the one covered with the plaster remained crack-free.

It is worth noting that the buildup of MgO particles on the inner wall of the plaster mould was found to be a relatively slow process when employing slip II (iPrOH as the solvent). This progression took around 6 min to achieve a thickness of 2.5 mm. In comparison, casting an alumina slip with water as the solvent achieved the same thickness in about 2 min, while zirconia took around 3 minutes. This phenomenon aligns

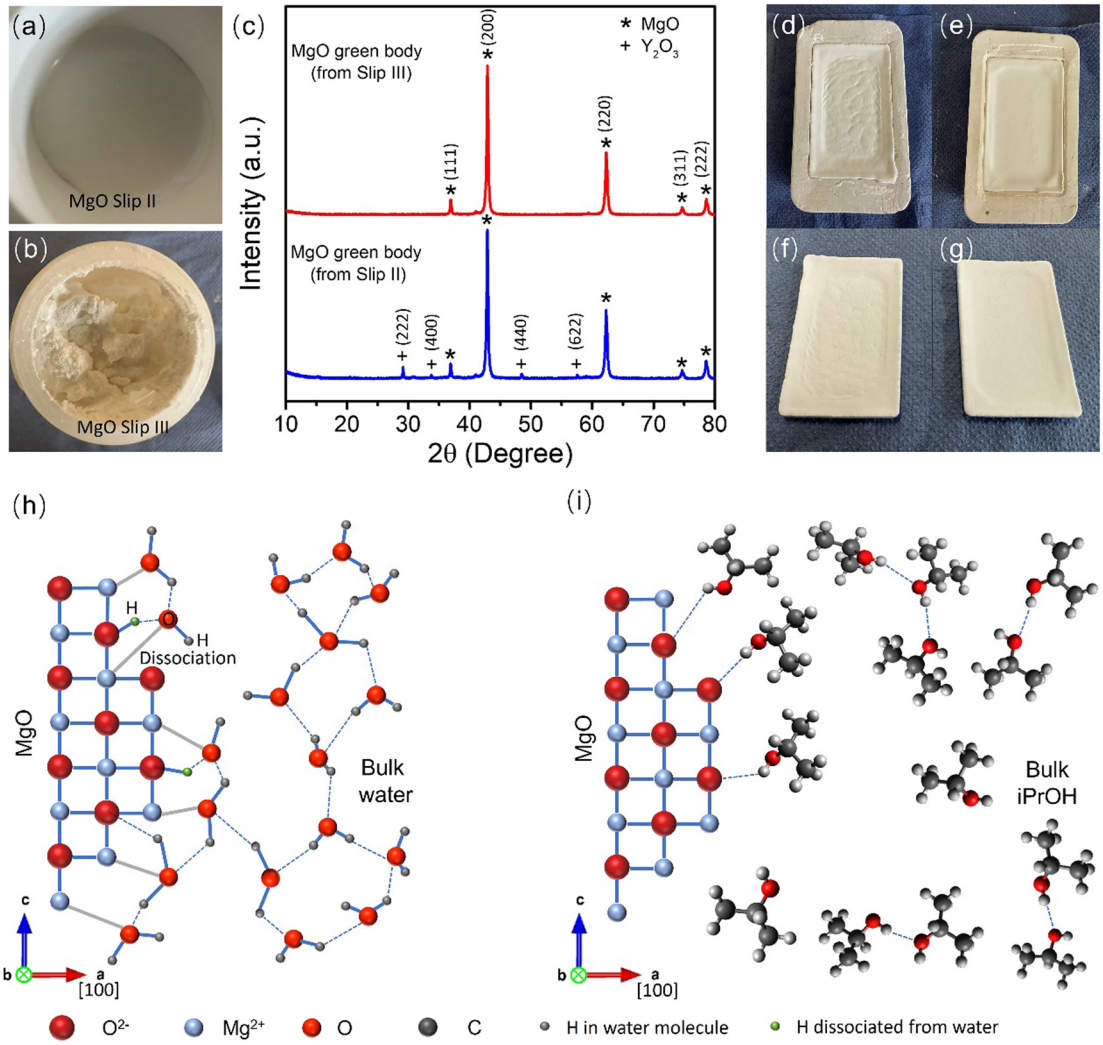

Fig. 3 Performance of slip II and slip III. (a) Photograph of slip II (iPrOH as liquid media). (b) Photograph of slip III (AcOH as liquid media). (c) XRD patterns of the MgO green bodies originating from slip II and slip III, XRD diffraction peaks corresponding to MgO and Y_2O_3 referenced to PDF No. 45-0946 and 43-1036. (d)–(g) Photographs of MgO crucible lids made from slip II (in green body state, with size of 79.2 mm by 8.5 mm by 3.8 mm). Slip casting process follows a standard operation procedure without a cover (d), (f) and an optimised operation procedure with a cover (e), (g). The MgO green bodies in (d) and (e) are depicted within the plaster moulds while those in (f) and (g) are shown after demoulding. Schematic diagrams of (h) water absorption and dissociation on the surface of a MgO particle and (i) interaction between iPrOH and the MgO particle surface. The MgO surface with steps depicted in (h) and (i) originates from raw MgO powder with a random rod-like morphology and the very outer atomic layer represents the (100) plane.

Table 1 Vapour pressure (kPa) of various solvents used in MgO slip formulations

Solvent	Vapour pressure (kPa)
Water	2.34 (20 °C)[46]
iPrOH	4.67 (21 °C)[47]
AcOH	1.57 (20 °C)[48]

with the findings of Oumizono *et al.*, although the casting rate reported in their study is even slower (3.78 mm in 2 hours).[26] The underlying cause of this phenomenon was not identified in their work. Here, we proposed that the difference in the rate of thickness buildup can be attributed to the varying rate at which the solvent enters the structure of the plaster mould. The porous microstructure of the plaster mould was expected to comprise numerous small capillaries and pores that could facilitate the spontaneous flow of liquid to fill these minute pathways. This capillary action is affected by the wettability of the liquid on the wall surfaces of the porous plaster mould. Water exhibits better wettability on a plaster mould than iPrOH. Consequently, water flows into the plaster at a faster rate than iPrOH, resulting in quicker MgO particles buildup on the plaster mould for water-based slip than for iPrOH.

To mitigate the rapid drying rate of the inner side by slowing down solvent evaporation, we sought an appropriate alternative and found acetic acid (AcOH) to be suitable. As indicated in Table 1, AcOH has a vapour pressure of 1.57 kPa. Notably, this value is considerably lower than that of iPrOH (4.67 kPa) and even lower than water (2.34 kPa). This low vapour pressure ensures a slow evaporation of solvent into the atmosphere,

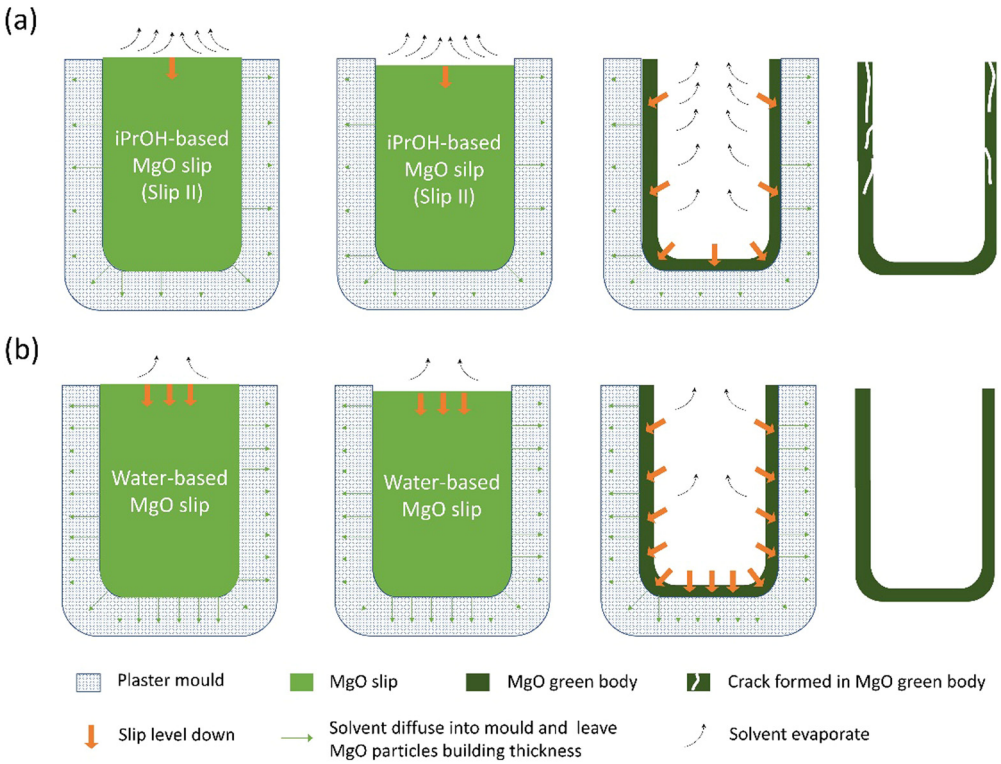

Fig. 4 Schematic diagrams depicting the slip casting processes using (a) an iPrOH-based MgO slip (slip II) and (b) a water-based MgO slip with favourable flowability.

which is anticipated to yield a better MgO slip casting performance compared to iPrOH.

However, the expected advantages did not realise due to an issue encountered during the slip preparation stage. Upon introducing the MgO powder into the AcOH liquid, which is termed as slip III, the dispersion generated heat and rapidly transformed from a liquid to a solid state, as depicted in Fig. 3(b). This swift change made it impossible to add the remaining MgO powder and other components. As a result, the corresponding XRD pattern in Fig. 3(c) for the MgO green body derived from slip III lacks the Y_2O_3 phase. The unanticipated heating of the slip is likely related to the reaction between hydration products and AcOH, according to reactions (4) and (5). The total reaction can be expressed by reaction (6). Because $(CH_3COO)_2Mg$ is hygroscopic, reaction (6) can occur in the reverse direction, and acetic acid may also evaporate during the two-day drying process under ambient conditions. Consequently, the XRD result does not reveal the presence of any impurities.

$$MgO + H_2O \rightleftharpoons Mg(OH)_2 \quad (4)$$

$$Mg(OH)_2 + 2CH_3COOH \rightleftharpoons 2(CH_3COO)_2Mg + 2H_2O \quad (5)$$

$$MgO + 2CH_3COOH \rightleftharpoons 2(CH_3COO)_2Mg + H_2O \quad (6)$$

Drawing from the findings presented earlier, the following criteria for selecting a suitable solvent to formulate an effective MgO slip are proposed:

a. The chosen solvent should exhibit low viscosity, promoting satisfactory flowability.

b. The selected solvent should not interact with MgO powders, thereby supporting efficient dispersion.

c. The vapour pressure of the solvent should not be excessively high (or the slip should be cast in a closed environment).

d. Good wettability on the plaster is desirable, enabling efficient capillary action and the easy penetration of the solvent into the porous plaster mould. After evaluating various common solvents, we cannot identify the one that outperforms either water or iPrOH. Employing a cover on the iPrOH-based slip can certainly slow down the evaporation rate on the inner side. However, it cannot effectively help with the buildup process on the outer side. Introducing a pressurised slip casting apparatus could potentially accelerate the penetration of iPrOH into the plaster mould, hence accelerate the MgO buildup on the mould walls. However, this approach was not explored in this study.

Interestingly, Allison had previously discussed the use of alcohol as a solvent in MgO slip casting in 1959,[40] and mentioned several drawbacks, including (1) a strong reliance on the skill of the operator during casting; (2) the high evaporation rate of alcohol leading to reduced process control; (3) challenges associated with demoulding; (4) rapid deterioration of the mould; and (5) limitations in producing large-sized MgO products. This work has overcome some of these challenges by employing iPrOH instead of alcohol.

3.3. Modification of the MgO slip through powder adjustment

In addition to altering the solvent to mitigate MgO hydration, another effective approach is to manipulate MgO powders. For example, it is possible to make the MgO powder less reactive and subsequently slow down the hydration kinetics.

It was found in this work that pre-firing could lead to the MgO powder becoming more rounded in shape, especially in comparison to its original state before firing. This transformation is evident from the SEM images displayed in Fig. 5. Furthermore, there was an observed increase in particle size after pre-firing, with the D50 value increasing from 0.79 μm to 1.58 μm. This size enlargement, as determined by SEM and particle size analysis, is likely to contribute to a slower reaction kinetics.

Kuenzel *et al.* proposed that MgO powders with smaller mean crystallite sizes, particularly those that are lightly burned, are more susceptible to hydration.[10] This is because the reactivity of MgO powders is significantly boosted when their crystallinity decreases. The $Mg(OH)_2$ layer on the surface of MgO can dissolve in the water layer and then reprecipitate as $Mg(OH)_2$ away from the surface. This exposes the underlying MgO to water, continuing the hydration process. Pan *et al.* also reported that the process of hydration and dehydration can lead to the aggregation and the cracking of MgO particles.[50] This is harmful for drying and sintering of the cast green body. It is worth noting that while larger particle sizes can be advantageous for suppressing hydration, they can also pose challenges in terms of dispersing effectively in water. This can impede achieving a homogeneous and stable dispersion.

Stoddard *et al.* adopted a different approach to managing MgO powders in their patent.[21] They utilised fused MgO powder with a particle size of <74 μm to create the slip. This MgO powder was mixed with water in a weight ratio of 10 : 3, and the slip was ball milled for 72 hours at 2–10 °C to reduce the hydration and decrease particle size during the milling process. Jones also employed MgO powders with a particle size of <74 μm in their slip casting process.[41]

Generally, a fine particle size (typically < 1 μm) is a desirable powder characteristic in producing advanced ceramics.[49] With a pre-firing temperature of 1000 °C, the particle size of MgO powder still falls within this range. Simultaneously, using the bottom-up strategy employed in this study consumes less time compared to the top-down strategy in casting an aqueous MgO slip as reported by Stoddard *et al.*

MgO powders before and after firing at 1000 °C were subjected to TGA in air, spanning from room temperature to 1100 °C. The commercial MgO powder contains absorbed water, loosely bound water, and $Mg(OH)_2$, with the overall water contents of 1.05, 1.66, and 1.34 wt%, respectively, which were determined *via* derivative weight plotting and the peak positions at 86 °C, 264 °C, and 362 °C, as illustrated in Fig. 6(a). The temperatures at which physically absorbed water was removed and $Mg(OH)_2$ decomposed align with the TGA outcomes reported by Pan *et al.*[50] However, the XRD analysis in Fig. 1(c) could not detect the presence of $Mg(OH)_2$ in the raw MgO powder, because its content (1.34 wt%, equivalent to1.89 vol%) was near the detection limit of XRD (1 vol%). Our TGA result confirms that the raw MgO commercial powder easily absorbs moisture even under ambient conditions, resulting in the formation of $Mg(OH)_2$. The active characteristic of raw MgO powders is responsible for the ice cream-like slip observed in Fig. 1(a), obtained by milling this powder with water for 16 hours.

The TGA curve for MgO powder pre-fired at 1000 °C did not display noticeable changes, and the weight change remains

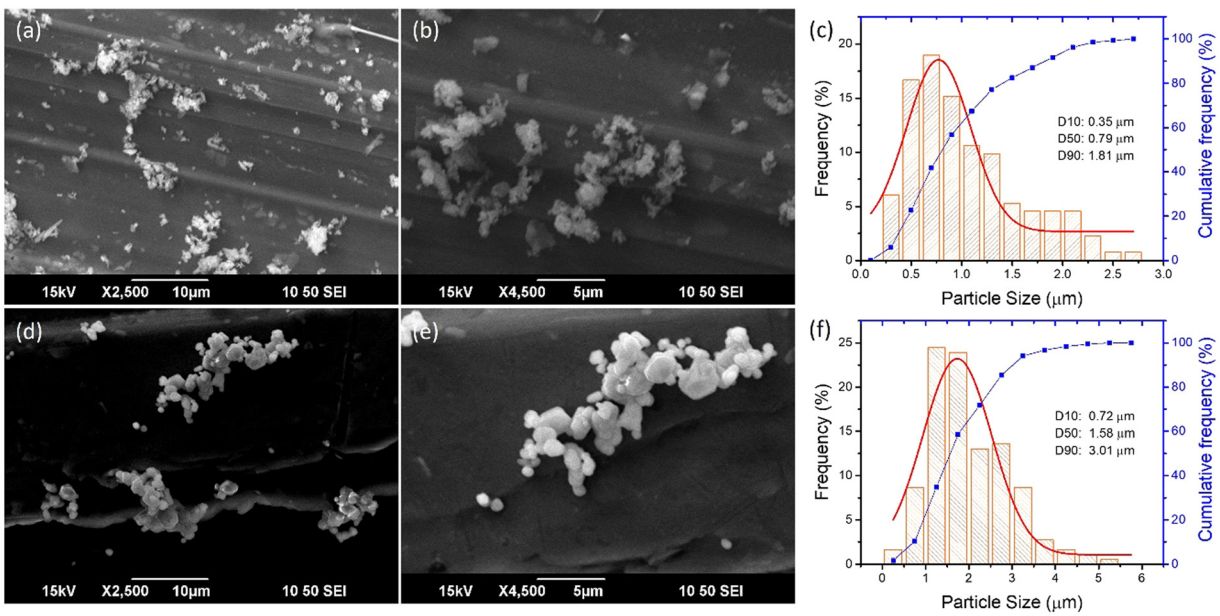

Fig. 5 SEM images of MgO commercial powders (a) and (b) before firing and (d) and (e) after firing at 1000 °C. Particle size distribution of MgO commercial powders (c) before firing and (f) after firing.

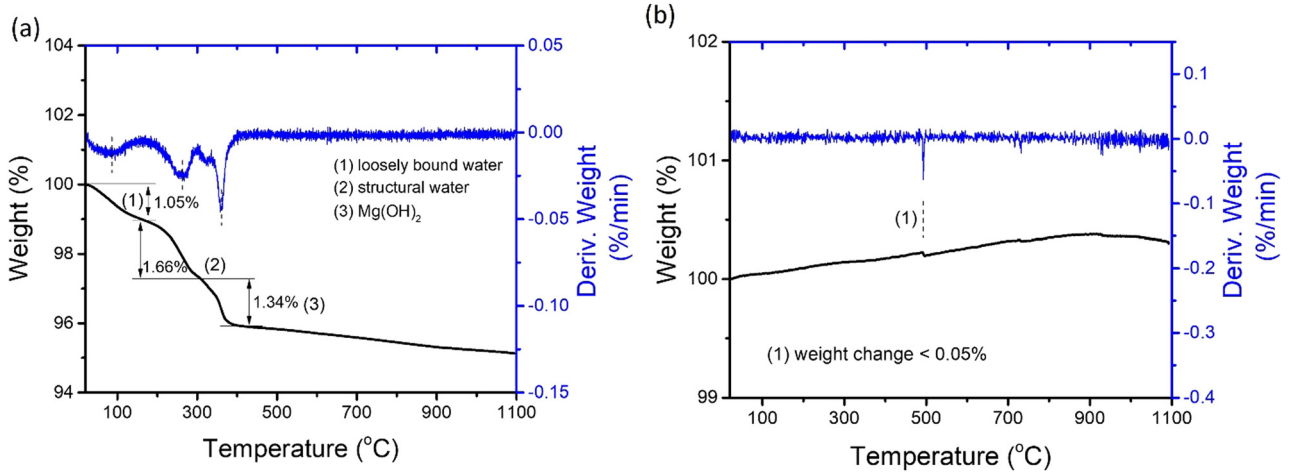

Fig. 6 Temperature-dependent mass recorded for (a) raw MgO powder and (b) MgO powder after firing at 1000 °C.

below 0.05% as shown in Fig. 6(b). This value is below the 0.1% verification threshold after calibration for the TGA instrument. The slight weight increase can be attributed to the reduction in buoyancy caused by decreased gas density at higher temperatures, consequently leading to a weight gain.

With regard to this pre-fired MgO powder, the TGA finding aligns with the XRD analysis, where only MgO and Y_2O_3 were detected, as illustrated in Fig. 7(c), validating that the firing process at 1000 °C enhanced the robustness of MgO powder. Pan *et al.*[50] investigated the thermal processes involving MgO hydration and the subsequent dehydration of $Mg(OH)_2$ at temperatures ranging from 300 to 700 °C, revealing that the amalgamation of MgO particles and a high temperature for dehydration contributed to reducing their reactivity. However, in our experiments, pre-firing the MgO powder at 500 °C for 4 hours and following the recipe of slip I did not result in a better slip compared to using the raw MgO powder (Fig. 1(a)). According to TGA results, $Mg(OH)_2$ should decompose at 500 °C. It appears that the presence of $Mg(OH)_2$ in the commercial powder is not the key factor affecting the slip behaviour.

A favourable slip (slip IV) was attained through the ball milling of the 1000 °C pre-fired MgO powder with water, as evidenced by the visual assessment depicted in Fig. 7(a). Slip IV demonstrated commendable flow characteristics with a viscosity of 54 mPa s, comparable to that of slip II (MgO slip based on iPrOH). After subjecting the mixture to a 16-hour ball milling process with water, the XRD patterns did not indicate the presence of $Mg(OH)_2$, in contrast to the original unfired MgO powder.

In addition to the increase in the particle size, the spherical morphology shown in Fig. 5(d) and (e) can also play a significant role in this substantial improvement. Ding and Selloni revealed that the water dissociation fraction on stepped surfaces

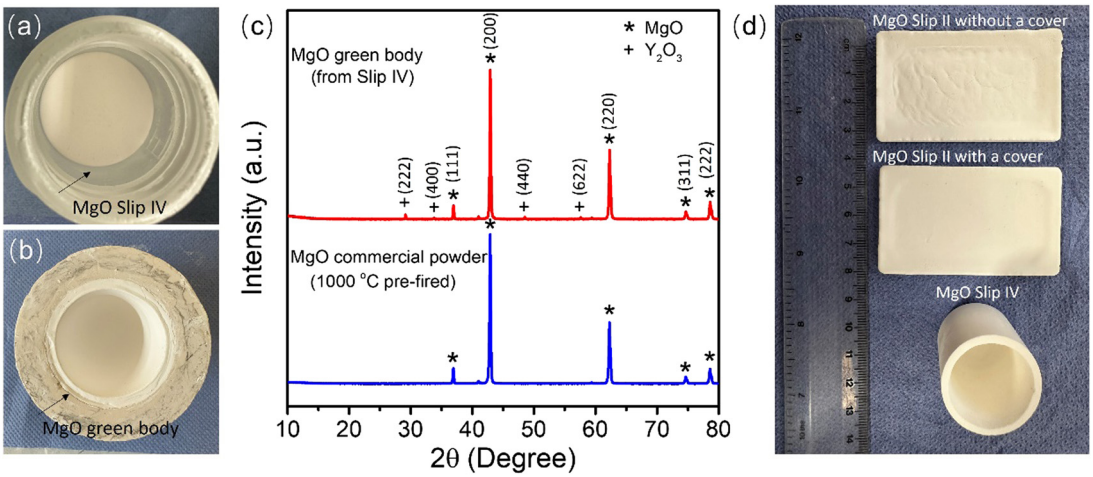

Fig. 7 Assessment and characterisation of slip IV. (a) Photograph of MgO slip IV (water-based). (b) photograph of the MgO green body drying in mould derived from slip IV (size: 35.4 mm in diameter and 41.2 mm in height). (c) XRD patterns of 1000 °C pre-fired MgO powder and the MgO green body originating from slip IV. XRD diffraction peaks corresponding to MgO and Y_2O_3 are referenced to PDF No. 45-0946 and 43-1036. (d) Final MgO products after sintering at 1610 °C derived from slip II and slip IV.

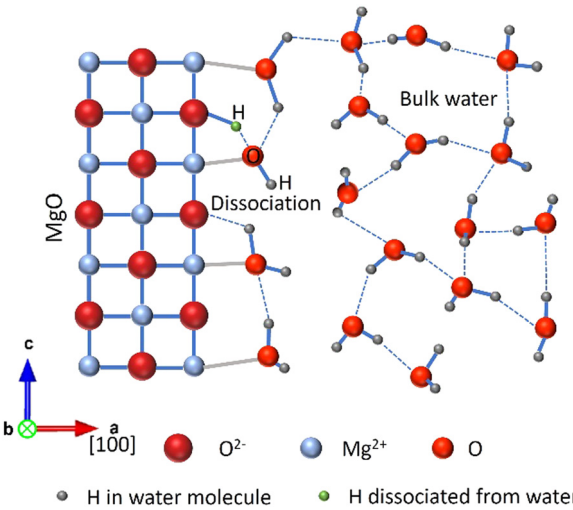

Fig. 8 Schematic diagram of water absorption and dissociation on the surface of a MgO particle. The flat MgO surface is derived from 1000 °C pre-fired MgO powder with a spherical morphology and the very outer atomic layer represents the (100) plane.

was higher compared to a flat surface.[42] Furthermore, according to a first principles study, Chen *et al.* predicted that the defective surface with low coordinated Mg atoms could be susceptible to hydration.[51] As shown in Fig. 5, the spherical morphology of the 1000 °C pre-fired MgO powder has fewer surface steps compared to the raw MgO powder, which exhibits a random rod-like morphology and a rough surface. Consequently, the interaction between water molecules and the MgO (100) plane becomes gentler and less intense, as illustrated in Fig. 8, compared to the interactions depicted in Fig. 3(h).

The green body of a MgO crucible produced using slip IV is presented in Fig. 7(b), displaying dimensions of 35.4 mm diameter and 41.2 mm height. After sintering at 1610 °C, the final product shown in Fig. 7(d) measured a diameter of 26.8 mm and a height of 31.9 mm, indicating a shrinkage of 23–24%. In the case of green bodies resulting from casting slip II, their initial dimensions are 79.2 mm by 8.5 mm by 3.8 mm, leading to a final size of 63.3 mm by 6.9 mm by 3.1 mm, with a shrinkage of 18–20%. The densities of the sintered MgO products derived from slip II and slip IV are listed in Table 2.

This powder adjustment method has proven to be effective for creating MgO products of small sizes. Current investigations are dedicated to improving the handling of a MgO slip by fine-tuning slip composition and the sequence of component mixing. This endeavour is aimed at bolstering the castability of MgO slips, resulting in a more manageable and reproducible slip casting process. In the pursuit of adapting slip casting for the fabrication of larger MgO products, successes have been realised, with achievements extending to a maximum volume size of 800 mL.

Table 2 Apparent density and relative density of sintered MgO products at 1610 °C, determined using Archimedes' method. The relative density is obtained by dividing the apparent density by the theoretical density which is 3.58 g cm^{-3}

Density	MgO product derived from slip II	MgO product derived from slip IV
Apparent density	3.37 g cm^{-3}	3.42 g cm^{-3}
Relative density	94.1%	95.5%

4. Conclusions

In this study, we successfully controlled the hydration in casting aqueous slips of MgO powder and fabricated MgO products with relative densities greater than 95% and purities exceeding 95 wt%.

Four different slips were formulated to explore the slip casting process of MgO and its hydration effects during casting. These slips were prepared using three different types of solvents or liquid dispersion media: water, isopropanol (iPrOH), and acetic acid (AcOH). We observed that solvents play a significant role in slip casting and proposed criteria for selecting the optimal solvent to produce high-quality MgO slips. These criteria include considerations of viscosity, vapor pressure, wettability on plaster, and reactivity towards MgO. We also found that water holds advantages over other solvents if the hydration issue can be resolved.

To control hydration, we modified the commercial MgO powder to make it suitable for creating aqueous slips. Initially, the powder contained absorbed and loosely bound water, along with a small quantity of $Mg(OH)_2$ formed during storage. This powder was highly reactive with water, leading to noticeable $Mg(OH)_2$ formation after 16 hours of ball milling at 5 °C. Subjecting the powder to firing at 1000 °C eliminated the absorbed water, decomposed the $Mg(OH)_2$, and promoted the growth of MgO particles (with D50 still in the range of <2 μm). This bottom-up strategy rendered the powder resistant to hydration and enabled the aqueous slip casting process to proceed smoothly and efficiently, delivering high-density and high-purity MgO products. However, the possibility of reducing the pre-firing temperature remains an open question. Further research is necessary to establish the relationship between the pre-firing temperature and the extent of hydration resistance in MgO particles.

Author contributions

Yu Yu was responsible for designing and conducting research, analysing data, and drafting the manuscript. Arkadiusz Gargala actively participated in the casting process and provided valuable insights and recommendations for MgO slip casting, while Michael Misson was in charge of overseeing the MgO casting process at Almath Crucibles Ltd. George Z. Chen played a pivotal role in supervising and coordinating the research activities conducted at the University of Nottingham and contributed to revising the manuscript.

Data availability

Data for this article, including XRD (txt), SEM (tif), TGA (txt), particle size analysis (txt), vesta drawing, and BET (pdf) are

available at figshare at **https://figshare.com/s/5e136b8552686ff4897f**.

Conflicts of interest

There are no conflicts to declare.

Acknowledgements

This work was supported by Almath Crucibles Ltd., the University of Nottingham, and Innovate UK (grant No. 10017140). This work contributed to Almath Crucibles Ltd. being awarded the King's Award for Enterprise in the innovation category in 2024. The authors thank the Nanoscale and Microscale Research Centre (nmRC) for providing access to instrumentation. The authors also thank Prof. Edward Lester and Dr Lei Lei of the Faculty of Engineering, University of Nottingham for kindly providing BET analysis, and engaging in valuable discussions, respectively.

References

1 K. Avarmaa, H. O'Brien, H. Johto and P. Taskinen, *J. Sustainable Met.*, 2015, **1**, 216–228.
2 W. Wang, L. Xue, T. Zhang, L. Zhou, J. Chen and Z. Pan, *Ceram. Int.*, 2019, **45**, 20664–20673.
3 M. J. V. Menken and A. A. Menovsky, *J. Cryst. Grow.*, 1988, **91**, 264–267.
4 Y. Kim, J. Yoo and J. Kang, *Metals*, 2020, **10**, 906.
5 K. Avarmaa, H. Johto and P. Taskinen, *Metall. Mater. Trans. B*, 2016, **47**, 244–255.
6 M. Maryška and J. Bláha, *Ceram. Silik.*, 1997, **41**, 121–124.
7 V. S. Birchal, S. D. F. Rocha, M. B. Mansur and V. S. T. Ciminelli, *Can. J. Chem. Eng.*, 2001, **79**, 507–511.
8 D. R. Glasson, *J. Appl. Chem.*, 1963, **13**, 119–123.
9 G. L. Smithson and N. N. Bakhshi, *Can. J. Chem. Eng.*, 1969, **47**, 508–513.
10 C. Kuenzel, F. Zhang, V. Ferrándiz-Mas, C. R. Cheeseman and E. M. Gartner, *Cem. Concr. Res.*, 2018, **103**, 123–129.
11 S.-H. Park, S.-m Jeon and J. Jang, *Characteristic Behavior of Hydration of Magnesium Oxide*, Springer, Singapore, 2020, pp. 1275–1279.
12 Z. Deng, Y. Wei, H. Zhou, K. Tuo, Y. Wang and Y. Zhang, *Int. J. Appl. Ceram. Technol.*, 2023, **20**, 1547–1556.
13 Z. Li, S. Zhang and W. E. Lee, *Int. Mater. Rev.*, 2008, **53**, 1–20.
14 V. Bagaria, *BTech Thesis*, National Institute of Technology Rourkela, 2012, 12–31.
15 T. Odatsu, T. Sawase, K. Kamada, Y. Taira, T. Shiraishi and M. Atsuta, *Dent. Mater. J.*, 2008, **27**, 251–257.
16 C. B. Abi, O. F. Emrullahog and G. Said, *J. Mech. Behav. Biomed. Mater.*, 2013, **18**, 123–131.
17 M. Abbasloo, H. Shokrollahi and A. Alhaji, *Mater. Chem. Phys.*, 2020, **254**, 123387.
18 M. M. Mahmoudabad and B. Hashemi, *Ceram. Int.*, 2019, **45**, 10400–10413.
19 J. G. Thompson and M. Mallett, *J. Res. Natl. Bur. Stand.*, 1939, **23**, 319–327.
20 S. Stoddard, D. Doll, J. Taub, D. Nuckolls, B. Shroyer, J. Rosenthal and T. Jones, *Casting of Magnesium Oxide in Aqueous Slips*, Los Alamos Scientific Laboratory, New Mexico, 1957, pp. 11–26.
21 S. D. Stoddard and D. E. Nuckolls, *US Pat.*, 3116155, 1963.
22 S. G. Whiteway, *J. Am. Ceram. Soc.*, 1963, **46**, 215–218.
23 L. Skomorovskaya, V. Zlatkovskii and I. Nemets, *Refractories*, 1991, **32**, 572–578.
24 L. A. Mondy, C. B. DiAntonio, T. P. Chavez, L. G. Hughes, A. Grillet, C. C. Roberts and D. T. Ingersoll, Creation and Characterization of Magnesium Oxide Macroporous Ceramics, Conference: Proposed for presentation at the 11th AIChE Annual Meeting, Minneapolis, 2011.
25 W. M. Silva, C. G. Aneziris and M. A. M. Brito, *J. Am. Ceram. Soc.*, 2011, **94**, 4218–4225.
26 H. Oumizono, T. Sasaki, H. Sasaki and H. Miyamoto, *J. Jpn. Soc. Powder Powder Metall.*, 1988, **35**, 614–618.
27 S. Köbel, D. Schneider and L. J. Gauckler, *Int. J. Mater. Res.*, 2003, **94**, 200–207.
28 S. G. Whiteway, M. Coll-Palagos and C. R. Masson, *Am. Ceram. Soc. Bull.*, 1961, **40**, 432–439.
29 Y. Xu, X. Mao, J. Fan, X. Li, M. Feng, B. Jiang, F. Lei and L. Zhang, *Ceram. Int.*, 2017, **43**, 8839–8844.
30 W. C. Mackrodt and R. F. Stewart, *J. Phys. C: Solid State Phys.*, 1979, **12**, 5015–5036.
31 G. Busker, M. A. van Huis, R. W. Grimes and A. van Veen, *Nucl. Instrum. Methods Phys. Res., Sect. B*, 2000, **171**, 528–536.
32 B. P. Uberuaga, R. Smith, A. R. Cleave, G. Henkelman, R. W. Grimes, A. F. Voter and K. E. Sickafus, *Phys. Rev. B: Condens. Matter Mater. Phys.*, 2005, **71**, 104102.
33 C. A. Gilbert, S. D. Kenny, R. Smith and E. Sanville, *Phys. Rev. B: Condens. Matter Mater. Phys.*, 2007, **76**, 184103.
34 J. Mulroue and D. M. Duffy, *Proc. R. Soc. A*, 2011, **467**, 2054–2065.
35 D. Alfè and M. J. Gillan, *Phys. Rev. B: Condens. Matter Mater. Phys.*, 2005, **71**, 220101.
36 A. De Vita, M. J. Gillan, J. S. Lin, M. C. Payne, I. Štich and L. J. Clarke, *Phys. Rev. Lett.*, 1992, **68**, 3319–3322.
37 F. Landuzzi, L. Pasquini, S. Giusepponi, M. Celino, A. Montone, P. L. Palla and F. Cleri, *J. Mater. Sci.*, 2015, **50**, 2502–2509.
38 D. Jiang and A. K. Mukherjee, *J. Am. Ceram. Soc.*, 2010, **93**, 769–773.
39 S. S. H. Seyedrazi and E. Taheri-Nassaj, *Mater. Chem. Phys.*, 2018, **219**, 96–108.
40 A. G. Allison, *US Pat.*, 2902380, 1959.
41 C. M. Jones, *US Pat.*, 3133792, 1964.
42 Z. Ding and A. Selloni, *J. Chem. Phys.*, 2021, **154**, 114708.
43 K. Jug, B. Heidberg and T. Bredow, *J. Phys. Chem. C*, 2007, **111**, 6846–6851.
44 J. P. Coulomb, B. Demirdjian, D. Ferry and M. Trabelsi, *Adsorption*, 2013, **19**, 861–867.

45 M. Odelius, *Phys. Rev. Lett.*, 1999, **82**, 3919–3922.
46 A. Wexler and L. Greenspan, *J. Res. Natl. Bur. Stand. A. Phys. Chem.*, 1971, **75**, 213–230.
47 I. M. Smallwood, *Handbook of Organic Solvent Properties*, Halsted Press, New York, 1996.
48 A. C. Dimian, C. S. Bildea and A. A. Kiss, *Applications in Design and Simulation of Sustainable Chemical Processes*, ed. A. C. Dimian, C. S. Bildea and A. A. Kiss, Elsevier, Amsterdam, 1st edn, 2019, ch. 13, pp. 483–519.
49 M. N. Rahaman, *Ceramic Processing and Sintering*, Marcel Dekker New York, United States, 2003.
50 Z. Pan and C. Y. Zhao, *Energy*, 2015, **82**, 611–618.
51 J. Chen, L. Huang, L. Dong, H. Zhang, Z. Huang, F. Li and S. Zhang, *Appl. Surf. Sci.*, 2023, **611**, 155441.